

# Characterization of the aircraft bay/landing gear coupling noise at low subsonic speeds and its suppression using leading-edge chevron spoiler

Advances in Mechanical Engineering  
2019, Vol. 11(8) 1–14  
© The Author(s) 2019  
DOI: 10.1177/1687814019871431  
journals.sagepub.com/home/ade  


Kun Zhao<sup>1</sup> , Yong Liang<sup>1</sup>, Tingrui Yue<sup>1</sup>, Zhengwu Chen<sup>1</sup> and Gareth J Bennett<sup>2</sup>

## Abstract

When the aircraft opens the bay door to let the landing gear either drop or retract, the incoming flow will result in a significant amount of coupling noise from the bay and the landing gear. Here, an experimental study was reported to characterise the acoustic performance and flow field at low subsonic speeds. Also, we examined a passive control method leading-edge chevron spoiler to suppress the noise. The experiment was performed in a low-speed aeroacoustic wind, the bay was simplified as a rectangular cavity and the spoiler was mounted to the leading edge. Both acoustic and aerodynamic measurements were performed through two microphone arrays, pressure transducers and particle image velocimetry. It was found that installation of the landing gear model can attenuate cavity oscillation noise to some extent by disturbing the shear layer of the cavity leading edge. Moreover, acoustic measurement confirmed the noise control when the spoiler was used. In addition, a parametric study on the effects of chevron topology was performed, and an optimised value was found for each parameter. From the aerodynamic measurement, the noise reduction was explained from the perspective of fluid dynamics. It was observed that installation of the chevron can raise the leading-edge shear layer and break up the large-scale vortices, thereby controlling the Rossiter mode noise and the landing gear model noise at certain frequencies.

## Keywords

Bay/landing gear, coupling noise, leading-edge chevron spoiler, low subsonic speeds, Rossiter mode, particle image velocimetry

Date received: 25 February 2019; accepted: 31 July 2019

Handling Editor: James Baldwin

## Introduction

The landing gear, which is designed to support an entire load of a landed aircraft on the ground, has been identified as a significant source of the airframe noise.<sup>1–5</sup> Besides, current landing gear is commonly retractable, that is, when not needed during flight, the undercarriages will retract into the wings or the fuselage, concealed behind doors. The space for concealing the retractable gears is termed as the landing gear bay.

<sup>1</sup>Key Laboratory of Aerodynamic Noise Control, China Aerodynamics Research and Development Center, Mianyang, P.R. China

<sup>2</sup>School of Engineering, Trinity College Dublin, The University of Dublin, Dublin, Ireland

### Corresponding author:

Kun Zhao, Key Laboratory of Aerodynamic Noise Control, China Aerodynamics Research and Development Center, Mianyang 621000, Sichuan, P.R. China.  
Email: zhaokun@cardc.cn



However, the bay can generate cavity noise when the incoming flow passes, regardless of the flow speed.<sup>6,7</sup>

Research on the landing gear bay noise can date back to the 1970s,<sup>8,9</sup> and the cavity oscillation has been recognised as the main characteristic of the noise generation. More specifically, when an incoming flow passes an open cavity, the separation occurs from the leading edge. The Kelvin–Helmholtz instability can result in vortices within the turbulent shear layer, which can develop and span to the whole length of the cavity opening. When it reattaches to the trailing edge, the impingement will radiate acoustic waves, propagating to all directions including the upstream. As they reach the front edge, the incident acoustic waves act as the perturbation and trigger the generation of other instabilities. This feedback mechanism will produce a few tones at different frequencies.<sup>10–12</sup>

Noise control of the landing gear and bay noise is an important research area in the aeroacoustic studies, and to date, a few approaches have been proposed to attenuate the landing gear or the bay noise (e.g. solid/perforated fairings<sup>13,14</sup> and air curtain<sup>15–17</sup> for the landing gear noise control, leading-edge spoiler<sup>18–21</sup> and fluid injection<sup>22,23</sup> for the cavity noise control). However, these techniques have not yet been tested to suppress the coupling noise of the landing gear and the bay.

The leading-edge chevron spoiler is a passive approach to suppress the cavity noise. It only involves geometric modification to the leading edge and does not require any external energy or mass input, therefore possessing much practical significance. The concept of using spoiler to reduce the cavity noise was first proposed by Rossiter,<sup>10</sup> who thought that spoiler can lift the shear layer and attenuate the impingement on the cavity aft wall. Until now, various spoilers with different topologies have been tested. Shaw et al.<sup>24</sup> performed one of the first attempts to use the chevron spoiler on a 4.9%-scaled F-111 generic weapon bay model, and the flow speed was managed to be within 0.7–2.0 Mach number. To date, it has been studied both experimentally and numerically by different researchers at high subsonic, transonic and supersonic speeds,<sup>19–21</sup> and good noise reduction was achieved. For low subsonic flow ( $Ma < 0.3$ ), the usefulness of the chevron spoiler has not yet been confirmed. However, this flow speed is of significance because for civil airline planes during take-off and approach, that is, the phases that annoy the airport vicinity, the landing gear is dropped out of the bay and the plane flies at low subsonic speeds. Moreover, as mentioned above, whether it works for the coupling noise of the bay, the landing gear also requires validation.

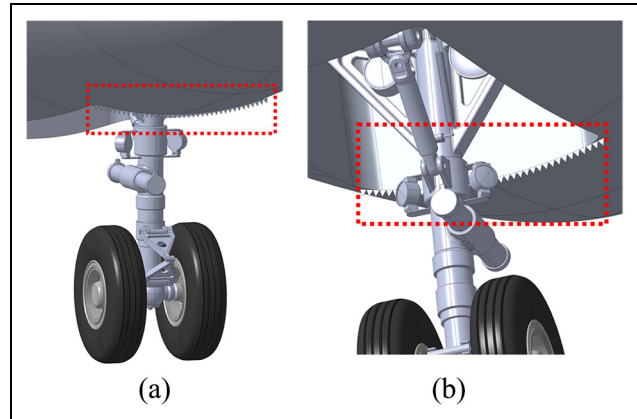


**Figure 1.** Schematic of the leading-edge chevron spoiler: (a) front view and (b) rear view.

In this article, characteristics of the bay/landing gear coupling noise at low subsonic conditions were discussed and leading-edge chevron spoiler was examined to suppress the coupling noise. Experiment was performed in a low-speed aeroacoustic wind tunnel. To characterise the coupling noise and its suppression, acoustic data from far-field microphones in a directivity arc array and a planar array were analysed. In addition, a set of fluctuating pressure transducers were mounted on the internal surface of the cavity, and particle image velocimetry (PIV) measurement was performed. Those results fundamentally explained the acoustic performance from a perspective of fluid dynamics.

### Concept of the leading-edge chevron spoiler

Concept of the leading-edge chevron spoiler is illustrated in Figure 1. The chevron topology consists of a number of adjacent identical isosceles triangles. As a passive control method, once installed to the leading edge of the landing gear bay, it is expected to result in perturbation to the bay leading-edge flow separation and the cavity oscillation, thereby suppressing the associated noise. Advantages of the chevron treatment can be summarised as follows: (1) ease of installation, (2) no cost of external energy or mass input, (3) no impedance to the maintenance and inspection of the landing gear or the bay and (4) almost no penalty of lift and little drag augment to the aircraft due to the small size.

### Experimental facilities and test program

In this study, the experimental work was performed using the facilities in China Aerodynamics Research

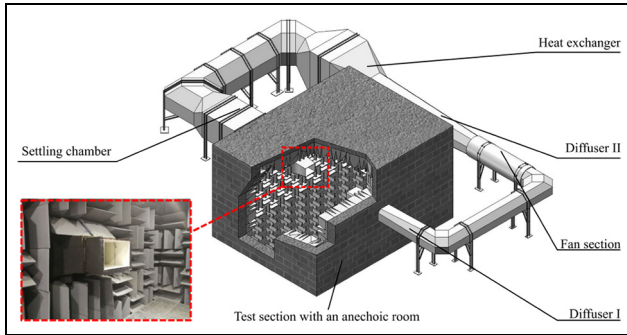


**Figure 2.** Configuration of 0.55 m  $\times$  0.4 m wind tunnel in CARDC.

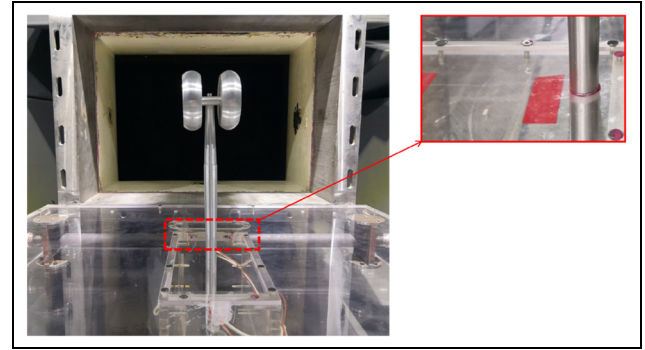


**Figure 4.** Picture of the landing gear set-up with the cavity covered.

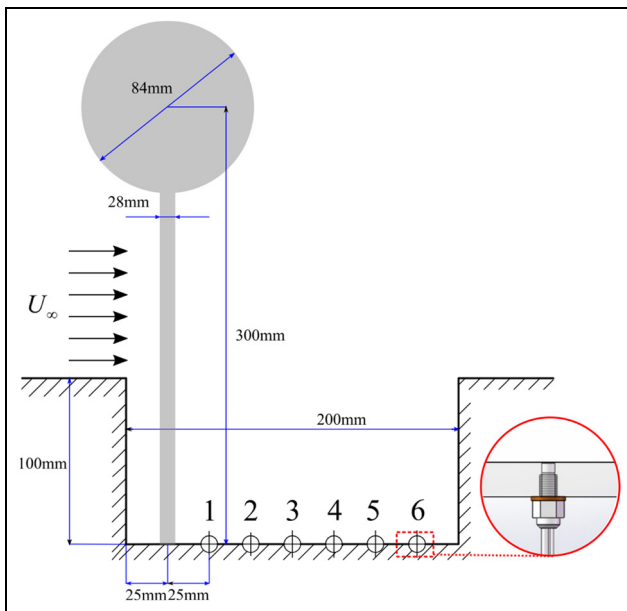


**Figure 3.** Installation schematic of the landing gear and the pressure transducers inside the cavity.

and Development Center (CARDC). In this section, details of the facilities, instrumentation and test program are reported.

### 0.55 m $\times$ 0.4 m wind tunnel

All tests were performed in the 0.55 m  $\times$  0.4 m small-scale aeroacoustics wind tunnel in CARDC. Here, 0.55 m  $\times$  0.4 m is the size of the nozzle outlet in the test section, at a height of 0.4 m. As illustrated in Figure 2, the wind tunnel is equipped with a full anechoic room (5.5 m  $\times$  3.7 m  $\times$  4 m) around the test section. The wind tunnel is powered by a 130 kW axial fan, allowing the main flow to be controlled within the range of 8–100 m/s, and the turbulence intensity in the core region is  $\leq 0.02\%$ . The wind tunnel outlet was equipped with a plexiglass end plate, flush with the lower side. All

models were installed on the end plate including the cavity and the landing gear.

### Bay/landing gear model

The landing gear bay was simplified as a rectangular cavity in this study, the size of which is 200 mm ( $l$ )  $\times$  100 mm ( $w$ )  $\times$  100 mm ( $d$ ). In addition to the bay, a two-wheel landing gear model was machined with aluminium. As illustrated in Figure 3, the model can be installed inside the cavity for the research on the coupling noise of the bay/landing gear. Installation of the pressure transducers is also depicted in Figure 3, with the dimension of the set-up provided. Specifically, the height of the main strut cylinder, that is, from the bottom of the cavity to the centre of the wheel, is 300 mm, and distance from the front wall to the cylinder is 25 mm. As to the wheel, the diameter is 84 mm. It is worth noting that when tests of the only landing gear noise were performed, the cavity was covered with a lid. A hole was drilled to let the strut go through, with the gap between them sealed by silicon to avoid additional noise, as depicted in Figure 4.

### Leading-edge chevron spoiler

The chevron spoiler consists of a base and isosceles triangles, as illustrated in Figure 5. There are three tapings left for the screws, and the spoiler was mounted to the front wall of the cavity. Note that the bottom of the triangles was flush with the leading edge; therefore, the bases did not contribute to the incoming flow perturbation. Rossiter<sup>10</sup> observed that the maximum tone suppression was achieved when the height of the spoiler was equal to the boundary-layer thickness in this rig. Therefore, it is inferred that dimension of the chevron has a significant effect on the noise control. As such, the triangles in the chevron were parametrized with three variables:  $a$ ,  $b$  and  $\alpha$ . Here  $a$  is the height and  $b$  is the width of each isosceles triangle, and  $\alpha$  is the

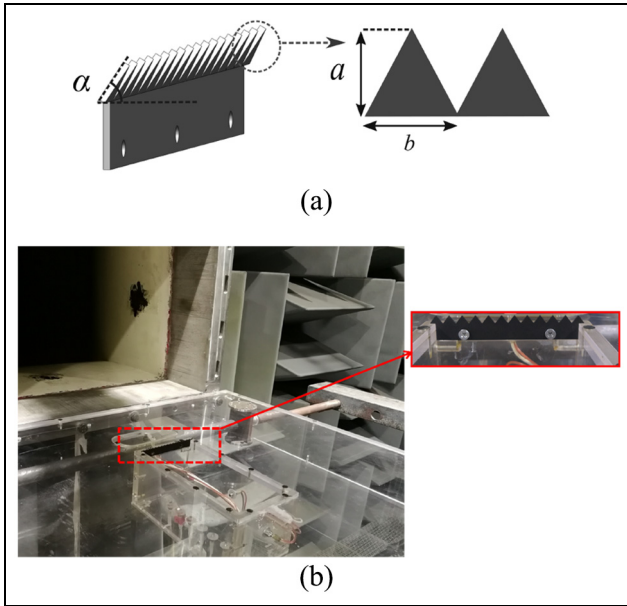


**Figure 5.** Leading-edge chevron spoiler: (a) topology and (b) installation.

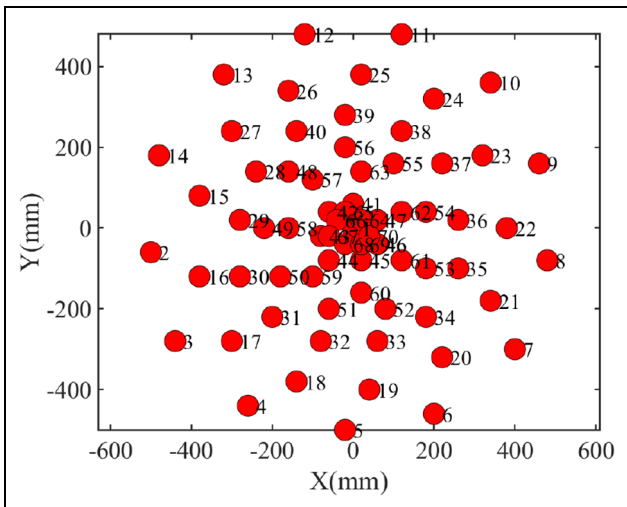


**Figure 6.** Pattern of the 70-microphone planar array.

inclination angle of each triangle relative to the upstream horizontal direction, as depicted in Figure 5(a). Therefore, when  $\alpha = 90^\circ$ , it means the chevron spoiler is vertical and when  $\alpha = 0^\circ$ , it means the chevron spoiler is flat. The installation set-up is shown in Figure 5(b). Parameters that were tested in this study will be reported in the subsequent section.

### Acoustic measurements

Acoustic measurements were performed through microphones in a planar array for noise localisation and an

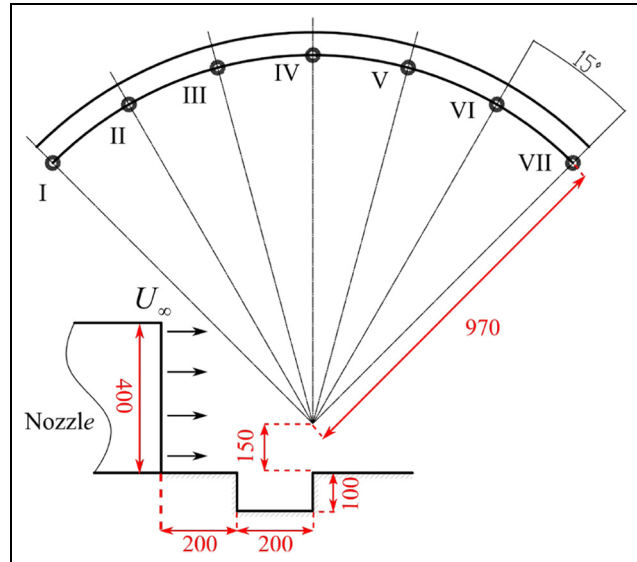


**Figure 7.** Schematic of the 7-microphone arc array installation.

arc array for far-field noise as well as sound directivity characterization.

**70-Microphone planar array.** The planar array consists of 70 microphones. Those microphones distribute in a spiral pattern, as depicted in Figure 6. One camera was attached in the centre of the array, allowing the beamforming noise localisation to be based on a real image. Distance from the microphone array to the reference plane, that is, the centre plane of the cavity, is 1.5 m. Data were processed with conventional beamforming, and the effects from the wind tunnel shear layer were corrected with the Amiet method.<sup>25</sup>

**7-Microphone arc array.** The far-field noise characteristics and sound directivity were evaluated using an arc array. The array consists of seven microphones, with an interval of  $15^\circ$ . Due to the fact that impingement of the separation flow to the trailing edge of the cavity is a direct source of the noise, centre of the arc aligned horizontally with the trailing edge, as illustrated in Figure 7. The arc array allows evaluating the noise directivity from  $-45^\circ$  to  $45^\circ$ . Note that the angle deviating from the vertical direction is termed as  $\phi$ , with downstream direction to be positive.

All microphones in those two arrays are 1/4-in G.R.A.S.<sup>®</sup> 46BE type with a dynamic range of 35 dBA–160 dB. The acoustic data, regardless of the planar or the arc array, were sampled at 51.2 kHz, and the sampling time was 30 s. Therefore, a total number of 1,536,000 sampling points were attained per channel. The data acquisition system was NI PXIe-1082, which allows the data from 77 microphones, that is, 70 from

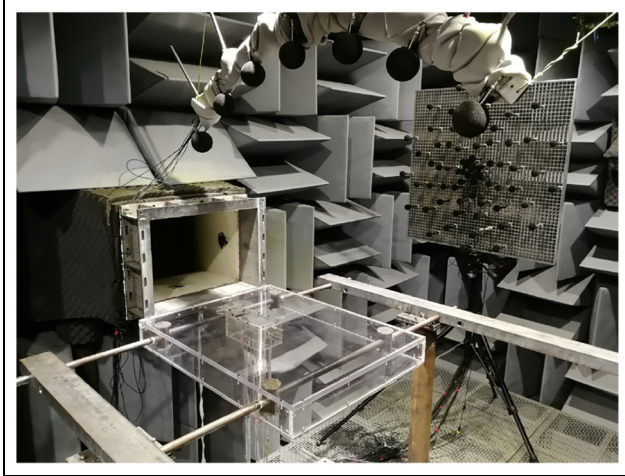


**Figure 8.** Set-up of the acoustic measurement.

the planar array and 7 from the arc array, to be sampled simultaneously (Figure 8).

### Pressure fluctuation

Pressure distribution inside the cavity along the bottom centreline was measured by seven piezoresistive pressure transducers in this study, as shown in Figure 3. All transducers were ENDEVCO® Model 8510B-2; the specification of which is given in English Units: the transducer has 10-32 mounting thread and 0.15-in face diameter; the measurement range is 0–2 Psi (1 Psi = 6.895 kPa), and the resonance frequency is 70 kHz. As shown in Figure 3, all transducers were mounted inside the tappings on the cavity ground, flush with the surface, and silicon was used to seal the gap. As shown in Figure 3, all tappings were spaced linearly with an interval of 25 mm. The same data acquisition system in the acoustic measurement was used so that the sampling frequency and the sampling time were 51.2 kHz and 30 s, respectively.

### PIV measurement

PIV is a useful measurement approach for visualising the flow field of the bay/landing gear in this study, thereby explaining the noise generation mechanism from a perspective of fluid dynamics. In this experiment, the LaVision® Time-Resolved PIV (TR-PIV) system was used, as shown in Figure 9. More specifically, a double-pulsed 30 mJ 532 nm neodymium-doped yttrium aluminium garnet (Nd:YAG) laser was fixed beside the test rig. The laser beam travels through an articulated arm to control the propagation direction. With a set of lenses inside, the articulated arm is also capable of scattering the laser into a sharp sheet, projecting from the top of the test platform. As depicted in

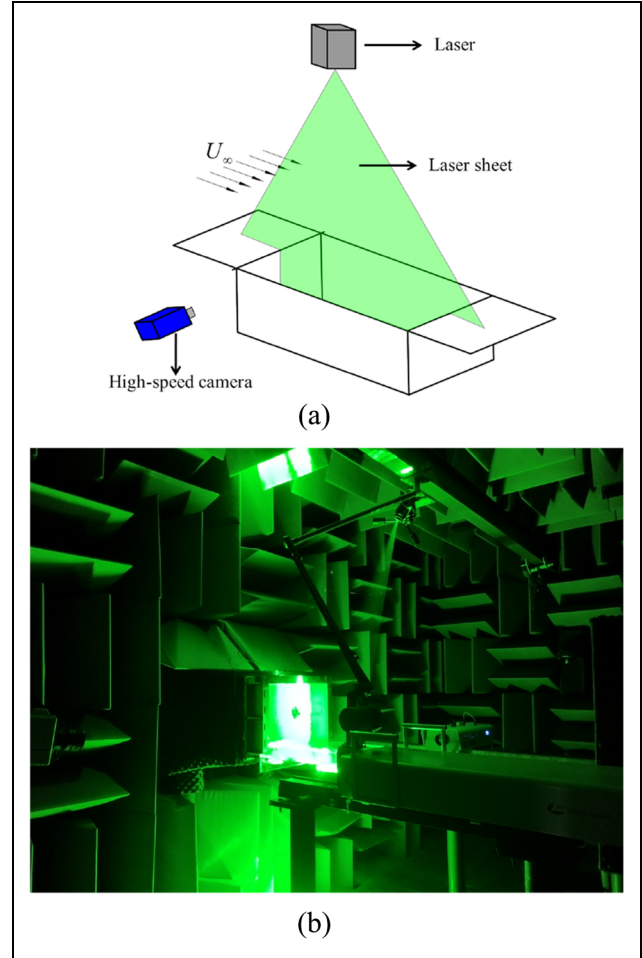


**Figure 9.** PIV set-up: (a) schematic and (b) picture view of the test.

Figure 9, the laser sheet aligns with the middle plane of the cavity, that is, the measurement plane. A HighSpeedStar Model CCD camera was mounted on the side of the test platform to capture image pairs with a resolution of  $1024 \times 1024$  pixels. The sampling rate was as high as 1.8 kHz, and for each running case, there are 1000 image pairs. The time interval between the paired images ( $dt$ ) is highly dependent on the flow speed; here,  $dt$  was set to be  $40 \mu\text{s}$  for  $U_\infty = 51 \text{ m/s}$  and  $30 \mu\text{s}$  for  $U_\infty = 85 \text{ m/s}$ . The image pairs were processed using cross-correlation in Davis 8.2 software with decreasing two-passes interrogation window sizes,  $48 \times 48$  and  $36 \times 36$ . The window overlap in each pass was 50%.

### Test program

In this study, a parametric study was performed to characterise the acoustic and aerodynamic performance of the flow regime. Test matrix is described in Table 1, with a Run No. distributed to each case. In each case, if

**Table 1.** Parameters of the test matrix.

Run No.	$U_\infty$	Cavity	LG	Chevron	$\alpha$	$a$	$b$	Case code
1	0.25 Ma	✓	×	×	—	—	—	Cavity
2	0.2 Ma	✓	×	×	—	—	—	Cavity
3	0.25 Ma	×	✓	×	—	—	—	LG
4	0.2 Ma	×	✓	×	—	—	—	LG
5	0.25 Ma	✓	✓	×	—	—	—	Cavity + LG
6	0.2 Ma	✓	✓	×	—	—	—	Cavity + LG
7	0.25 Ma	✓	×	✓	0°	3 mm	3 mm	Cavity + Chevron
8	0.25 Ma	✓	×	✓	30°	3 mm	3 mm	Cavity + Chevron
9	0.25 Ma	✓	×	✓	60°	3 mm	3 mm	Cavity + Chevron
10	0.25 Ma	✓	×	✓	90°	3 mm	3 mm	Cavity + Chevron
11	0.25 Ma	✓	×	✓	120°	3 mm	3 mm	Cavity + Chevron
12	0.25 Ma	✓	×	✓	150°	3 mm	3 mm	Cavity + Chevron
13	0.25 Ma	✓	×	✓	90°	3 mm	6 mm	Cavity + Chevron
14	0.25 Ma	✓	×	✓	90°	3 mm	9 mm	Cavity + Chevron
15	0.25 Ma	✓	×	✓	90°	6 mm	3 mm	Cavity + Chevron
16	0.25 Ma	✓	×	✓	90°	9 mm	3 mm	Cavity + Chevron
17	0.25 Ma	✓	✓	✓	90°	3 mm	3 mm	Cavity + Chevron

LG: landing gear.

there exists the component, for example, cavity, landing gear model (also termed as LG hereinafter) or leading-edge chevron spoiler (termed as Chevron), the corresponding grid in the table will be populated with a '✓'; otherwise, a '×' will be there instead. Note that if the Chevron exists, its parameters will also be provided, that is,  $\alpha$ ,  $a$  and  $b$ . Two Mach numbers were tested in this study for  $U_\infty$ : 0.25 and 0.2. They correspond to 85 and 68 m/s, respectively. In addition, a case code was provided to each case to help the readers quickly understand the set-up in the remainder of this article.

## Results and discussion

In this section, results and discussion will be provided based on the experiment mentioned above.

### Coupling noise and flow of the cavity and LG model

When the landing gear falls out of the bay, the flow field of these two parts will be coupled and so will be the noise. Here, characteristics of the coupling noise and flow are discussed based on the simplified landing gear model and the rectangular cavity.

**Characterization of the coupling noise.** Figure 10 illustrates the A-weighted 1/3 octave band spectra of those cases related to the coupling noise at two Mach numbers. The spectra were attained from Microphone No. IV in the arc array, that is,  $\phi = 0$ , and the cases include Cavity (No. 1 and No. 2), LG (No. 3 and No. 4) and Cavity + LG (No. 5 and No. 6). Note that the spectra almost overlap with each other below 315 Hz, which means the background noise dominates here. As such,

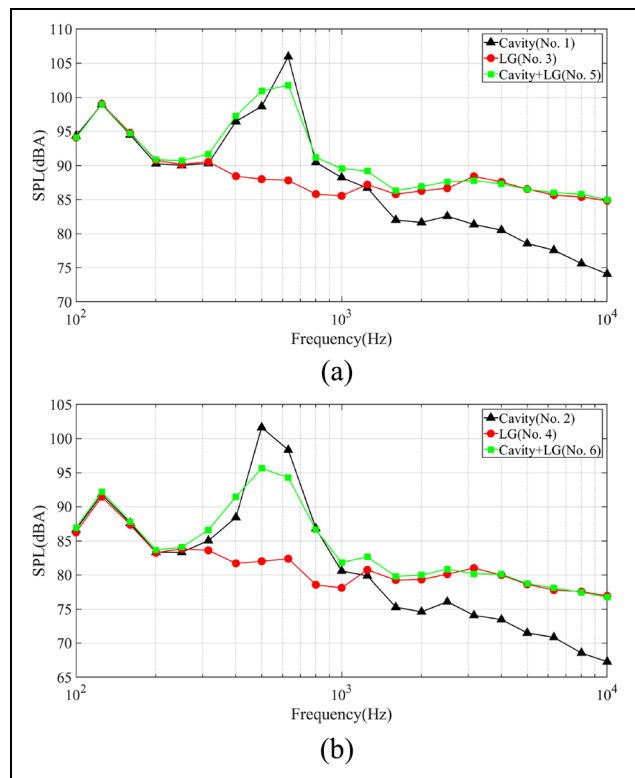


**Figure 10.** A-weighted 1/3 octave band spectra of cavity, LG model and coupling noise: (a) 0.25 Ma and (b) 0.2 Ma.

discussion on this range was not performed in the remainder of this article. For Cavity, that is, No. 1 and No. 2, one main tone can be observed in the low-frequency range of <1000 Hz. Besides, when Mach number changes, apart from sound pressure level

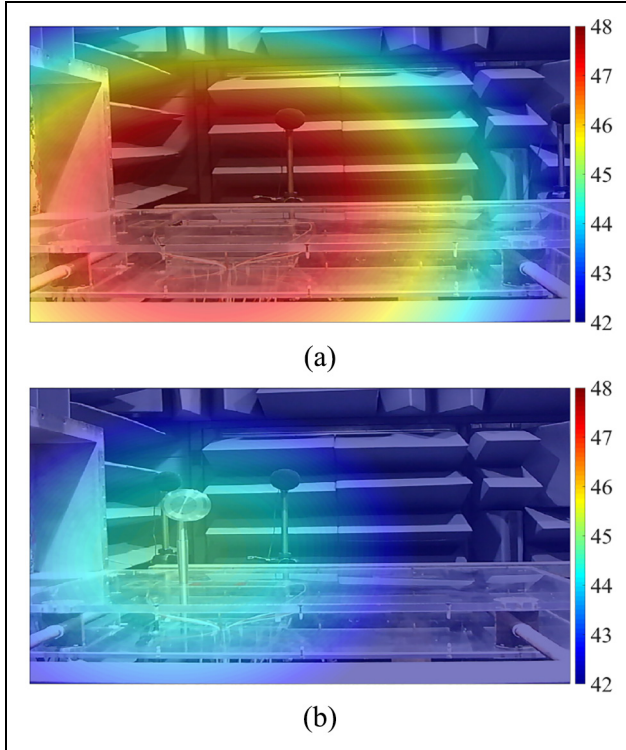


**Figure 11.** Noise localisation based on conventional beamforming at 900 Hz ( $U_\infty = 0.25$ ): (a) Cavity (No. 1) and (b) LG (No. 3).

(SPL), the main tone also moves to a different frequency. This suggests that the tone is from the Rossiter shear layer mode,<sup>10</sup> which is highly dependent on  $U_\infty$ . By comparison, the main tone disappears in the LG cases (No. 3 and No. 4) but SPL significantly increases in the frequency range of  $\geq 1600$  Hz. This means that the landing gear model produces more noise in high-frequency range ( $\geq 1600$  Hz) than the cavity, while the cavity is more active in low-frequency range ( $< 1000$  Hz).

The conclusion stated above can be further confirmed by beamforming. Figures 11 and 12 show the noise localisation results at 900 and 8000 Hz, respectively, with  $U_\infty$  of 0.25 Ma. First of all, it is worth noting that performance of the resolution at the low frequency of 900 Hz is not as good as the high frequency of 8000 Hz, which is a common disadvantage of the conventional beamforming. However, the peak of the contour is still able to demonstrate where the main noise source is. In Figure 11, the cavity is observed to produce higher SPL than LG at 900 Hz. By contrast, LG shows higher SPL at 8000 Hz than Cavity in Figure 12, and the peak occurs around the wheels. Therefore, noise localisation is in good agreement with what the A-weighted 1/3 octave band spectra demonstrated.

In Cavity + LG, characteristics of the coupled noise show distinct performance from the individuals. To be

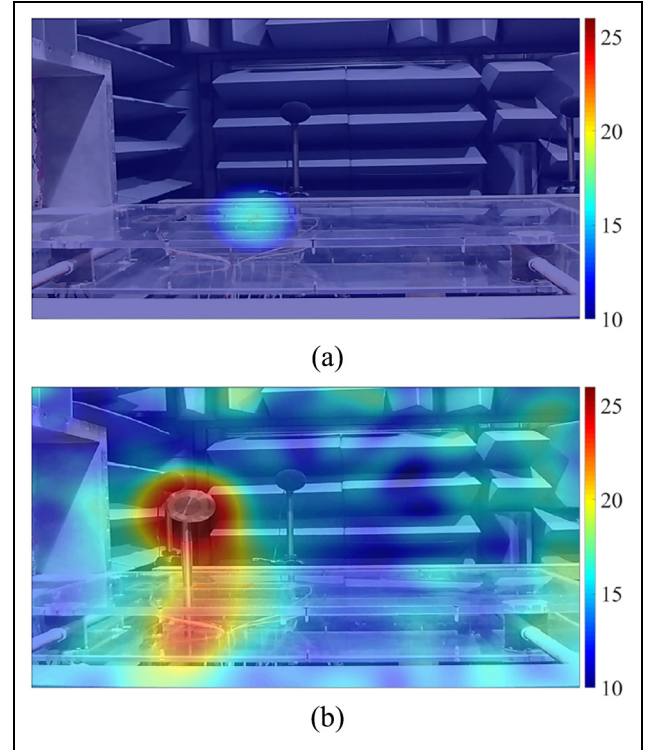


**Figure 12.** Noise localisation based on conventional beamforming at 8000 Hz ( $U_\infty = 0.25$ ): (a) Cavity (No. 1) and (b) LG (No. 3).

more specific, spectra of the cases with Cavity + LG (No. 5 and No. 6) in Figure 10 own a peak at the same frequency with Cavity cases, but SPL is a bit lower. This is inferred to be attributed to disturbance from LG to the cavity Rossiter shear layer mode. More specifically, when the shear layer separates from the front edge, it will impinge on LG strut instead of reaching the cavity aft wall, so the feedback loop cannot be established. Note that this disturbance only occurs in the middle because the shear layer beside the LG remains to interact with the cavity aft wall, which also explains why the peak still exists but SPL reduces. By contrast, noise in the high-frequency range ( $\geq 1600$  Hz) rises like the LG cases. Since noise in this frequency range is mainly from the wheels, which are not affected by the shear layer, the corresponding performance of LG and Cavity + LG is similar. In addition, it is observed that, for example, at 0.25 Ma, SPL of Cavity + LG is higher than LG at some frequencies, for example, 1250 Hz. This can be explained by the impingement of the shear layer to the landing gear main strut. For LG, the flow impinging on the strut is  $U_\infty$ ; by contrast, when the cavity exists, the leading-edge shear layer will impinge on the strut. It consists of large-scale vortices and results in more noise than  $U_\infty$ .

Conclusions can be further confirmed by the narrow-band spectra, as shown in Figure 13 at  $Ma = 0.25$ . The

spectra were attained from the same microphone in Figure 10. It is observed that when there is only the cavity, the peak stays at 650 Hz, while after the landing gear is assembled, the peak still stays there but goes lower. Besides, the frequencies predicted by the Rossiter equation have also been illustrated. The equation is expressed as follows<sup>10</sup>

$$St_n = \frac{f_n l}{U_\infty} = \frac{n - \alpha}{Ma + 1/\kappa} \quad (1)$$

where  $St_n$  and  $f_n$  are Strouhal number and frequency of the  $n$ th Rossiter mode, respectively;  $\alpha$  and  $\kappa$  were set to be 0.25 and 0.66, respectively.<sup>26</sup> Predicted frequencies of the second, third and fourth Rossiter modes are provided; it is found that those tones corresponding to the Rossiter oscillation can be reduced but still exist after the landing gear is added. All findings in the narrowband spectra are in good agreement with Figure 10.

When it comes to sound directivity as well as the overall sound pressure level (OASPL), A-weighted results from the microphone arc array are shown in Figure 14. First of all, regardless of Mach number and direction, it is observed that OASPL ranking is Cavity > LG > Cavity + LG. This suggests that the bay may produce more noise than the landing gear itself and the assembly of the two. In terms of the directivity, it is found that for LG, the peak appears at  $\phi = 30^\circ$  for both Mach numbers, while for Cavity, the peak appears at  $\phi = -15^\circ$  when Mach number is 0.25 Ma, and the peak appears at  $\phi = 15^\circ$  when Mach number is 0.2 Ma. This means that the performance of the cavity noise directivity is dependent on the incoming flow speed.

**Characterization of the coupling flow field.** Figures 15 and 16 show the instantaneous streamlines of the flow field at 0.25 Ma, achieved from PIV of Cavity (No. 1) and Cavity + LG (No. 5), respectively. Contour of the streamlines corresponds to the local flow speed, and

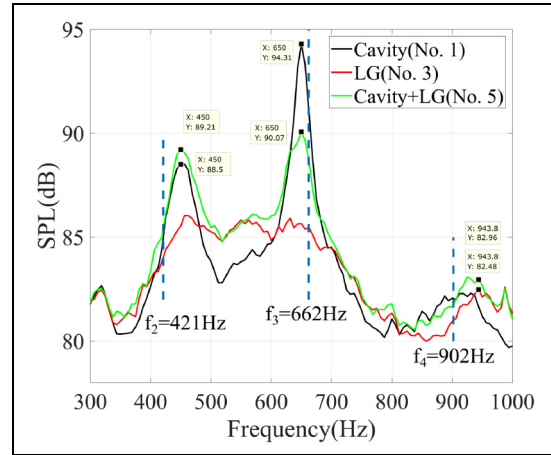


Figure 13. Narrowband spectral of cavity, LG model and coupling noise at 0.25 Ma.

those streamlines are superimposed on the greyscale image of Cavity (or Cavity + LG) to illustrate the relative position. As shown in Figure 15, vortices with different sizes show up in the flow field. Those, who are deep inside the cavity possess a large size, can be attributed to the recirculation flow of the cavity. By contrast, those, who have a small size and close to the lower side of the leading-edge shear layer, are the vortices due to the Kelvin–Helmholtz instability of the leading-edge shear layer. Note that no matter how small or large all those vortices are, they are all termed as large-scale vortices because those small-scale vortices cannot be visualised by PIV. The ‘large size’ and ‘small size’ mentioned here only refer to the relative scale. When those leading-edge vortices are transported to the aft wall, as illustrated in Figure 15(c), for example, the impingement will break them up and result in acoustic pressure, which is the origin of the Rossiter feedback. It is worth pointing out that after the authors carefully reviewed all instantaneous streamline images at different Ma numbers for Cavity cases (No. 1 and No. 2), no

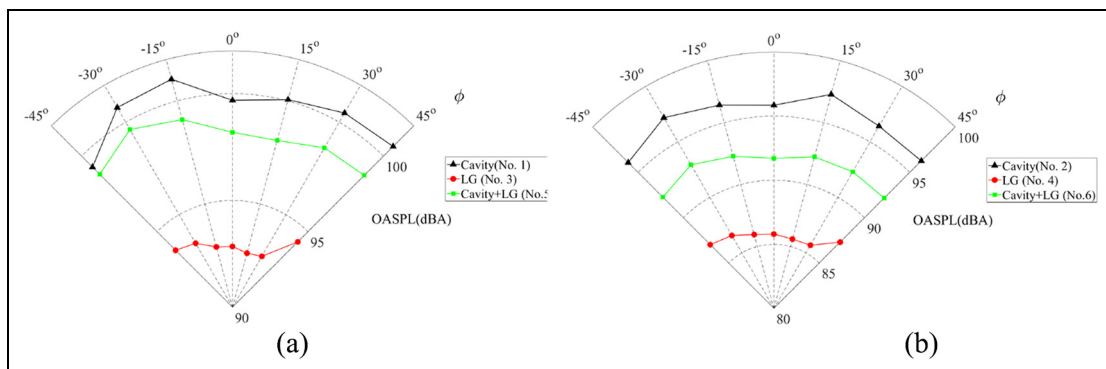
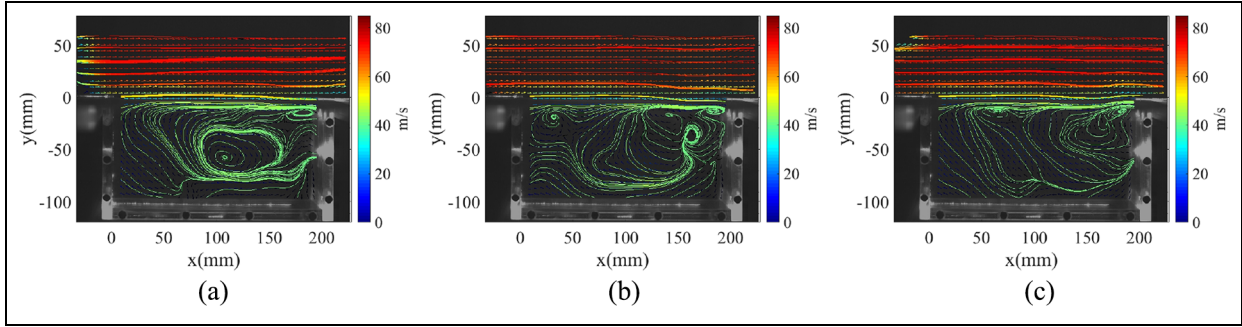
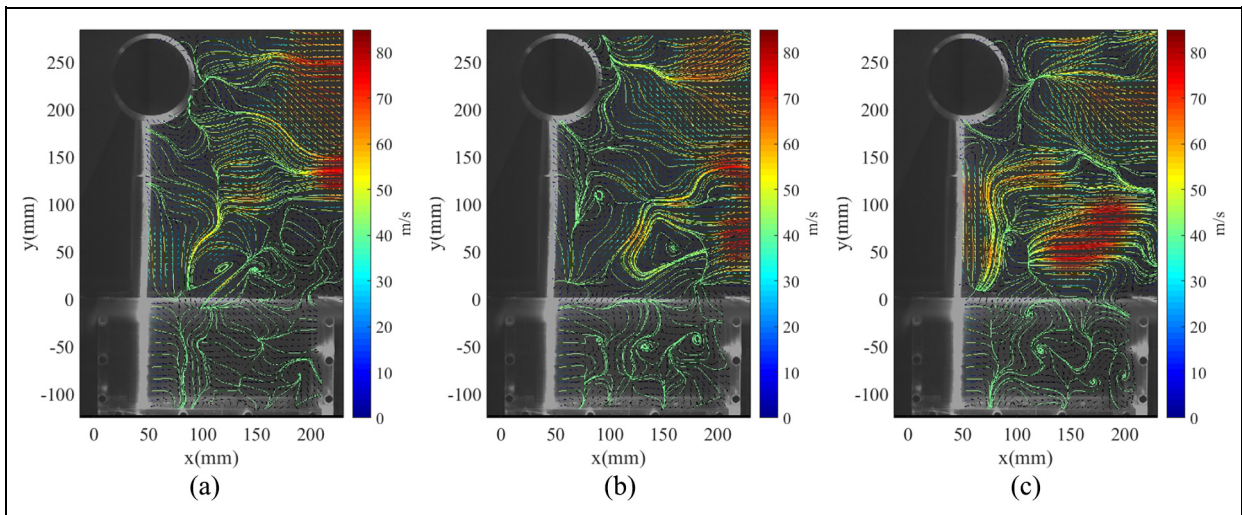


Figure 14. A-weighted OASPL directivity of cavity, LG model and coupling noise: (a) 0.25 Ma and (b) 0.2 Ma.





**Figure 15.** Examples of PIV instantaneous streamlines of the Cavity only case (No. 1) at 0.25 Ma.



**Figure 16.** Examples of PIV instantaneous streamlines of the Cavity + LG case (No. 5) at 0.25 Ma.

any obvious vortices above the upper edge of the leading shear layer were observed. This is because when such vortices occur, they are confronted with strong incoming flow, that is,  $U_\infty$ , which will tear them up immediately into much smaller sizes. Due to the resolution of PIV, they cannot be visualised either. By contrast, the flow speed below the shear layer in the cavity is much lower, as clearly illustrated in Figure 15, thereby allowing those vortices evolve and reach the aft wall.

Figure 16 provides the flow field of Cavity + LG. Compared with Figure 15, the significant difference confirms that the introduction of the landing gear model to the cavity can substantially affect the flow field. However, PIV results here only visualise the plane in the middle, not the side of the cavity. As pointed out earlier, the flow field of the cavity on the side should remain almost the same as that when there is no LG. Regarding results here, first of all, it is found that the shear layer disappears due to the blockage from the landing gear cylinder, and so does the corresponding

vortices. This fundamentally explains why the peak of the spectra reduces when comparing Cavity + LG (No. 1 and No. 2) with Cavity (No. 5 and No. 6) in Figure 10. Moreover, vortices can be detected not only inside the cavity but also over it. Considering their distinct appearance, size and occurrence area from those in Figure 15, those vortices are results of the flow separation from the strut. In addition, a number of stagnation points can be found, where some streamlines end and others start. This can be explained by the three-dimensional (3D) characteristics of the flow regime.<sup>27</sup> More specifically, fluid from other planes can enter the measurement plane and some inside can leave the measurement plane. This also explains why the flow speed in the area far behind the strut substantially increases, that is, more fluid from the main stream with higher speed on the side enters the measurement plane.

The pressure distribution inside the cavity is also discussed here because it is an important flow characteristic of the bay. For example, a steep pressure gradient established on the cavity floor for some geometries can

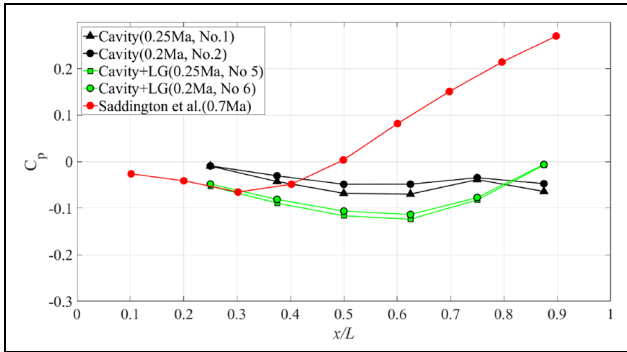


**Figure 17.** Mean pressure coefficient distribution of the cavity with or without landing gear model. Data from Saddington et al.<sup>20</sup> were also reported for comparison.

be unfavourable for store release, and it is therefore pertinent to reduce the gradient established along with the suppression of flow.<sup>20</sup> In this article, the pressure distribution along the bottom of the cavity is analysed by those transducers mentioned earlier. More specifically, the pressure coefficients of the cavities with and without the landing gear model are shown in Figure 17, calculated by the mean pressure divided by the incoming flow dynamic pressure. In Figure 17, for Cavity,  $C_p$  is below zero and decreases from upstream to downstream until close to the aft wall. A local peak can be detected around the second right transducer and then  $C_p$  decreases again. In terms of the pressure gradient, it cannot be described as ‘being steep’, at least not as steep as the data reported in the study by Saddington et al.,<sup>20</sup> which is also shown in Figure 17. However, the size and Mach No. of the test by Saddington et al.<sup>20</sup> are different from this study, that is, 320 mm ( $l$ )  $\times$  160 mm ( $d$ )  $\times$  64 mm ( $w$ ) and 0.7 Ma. Considering  $C_p$  at two Mach numbers almost falls at the same line in the experiment in this study, which means the flow speed has little impact on the mean pressure coefficient distribution, it is inferred that the coefficient pressure distribution is highly dependent on the size of the cavity. Since the size of cavity was kept to be constant in this study, their correlation is not discussed in detail here.

After the landing gear model is installed in the bay, whether it can substantially affect the pressure field inside the cavity is worth addressing. In Figure 17, the pressure coefficient of Cavity + LG is found to be only slightly lower than Cavity except the one most close to the aft wall, and the trend is similar as well. This can be explained by the 3D characteristics of the regime as well. To be more specific, the blockage by LG strut in the middle reduces the pressure level in the downstream field, with a pressure gradient generated in the spanwise direction. However, the gradient can be soon offset by those flow aside so that the pressure field inside the cavity farther downstream will not be affected much. This

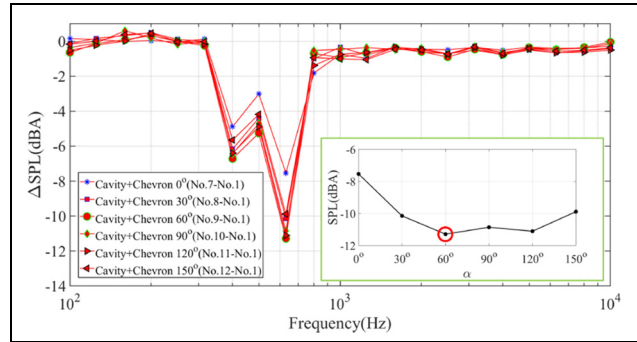


**Figure 18.** A-weighted  $\Delta$ SPL spectral of those tests with different  $\alpha$ .

suggests that if the cylinder is small compared to the width of the cavity, only minor variation occurs in the pressure field of a cavity when the landing gear is added.

### Noise suppression using leading-edge spoiler

Here, the noise suppression for both cavity and the coupling noise is discussed.

**Characterization of the cavity noise reduction.** First of all, effects of  $\alpha$  on the noise reduction were investigated. Figure 18 reports  $\Delta$ SPL spectra of those cases that correspond to Cavity + Chevron with different inclination angles. The incoming flow speed is 0.25 Ma, and the data were attained from Microphone No. IV as well. Note that  $\Delta$ SPL here is SPL subtraction of Cavity from Cavity + Chevron. Accordingly, if the value is positive, it means the noise level increases and vice versa.

As shown in Figure 18,  $\Delta$ SPL is negative for all cases over the frequency range greater than 315 Hz. It can be clearly observed that the maximum was achieved at the frequency of the Rossiter modes. This confirms that the chevron spoiler is able to suppress the Rossiter mode noise. In addition, the maximum reduction of each case with different  $\alpha$  is also reported as a line graph within Figure 18. The best performance is found to be achieved as  $\alpha = 60^\circ$  while the worst performance is found to be achieved as  $\alpha = 0^\circ$ .

The overall acoustic performance of the spoiler was analysed, as well as the sound directivity. Figure 19 shows A-weighted  $\Delta$ OASPL achieved from those microphones in the arc. Similarly, a negative value means noise reduction was achieved. It is observed that noise suppression exists in all cases with the chevron leading-edge spoiler, regardless of different  $\alpha$  and  $\phi$ . This further confirms its noise control ability from the perspective of overall acoustic performance. Moreover,  $\alpha = 60^\circ$  still shows best performance in terms of the

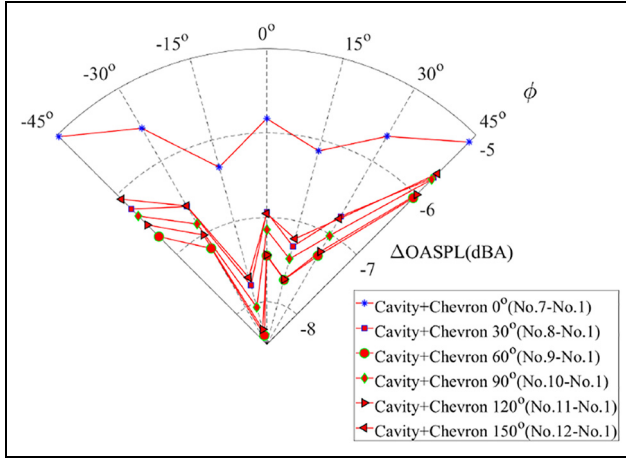


**Figure 19.** A-weighted  $\Delta$ OASPL directivity of the noise reduction, achieved using chevron with different  $\alpha$ .

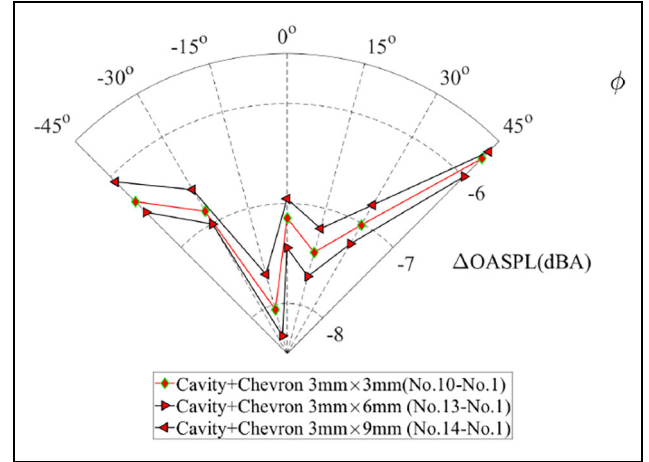


**Figure 21.** A-weighted  $\Delta$ OASPL directivity of the noise reduction, achieved using chevron with different  $b$  ( $\alpha = 90^\circ$ ).

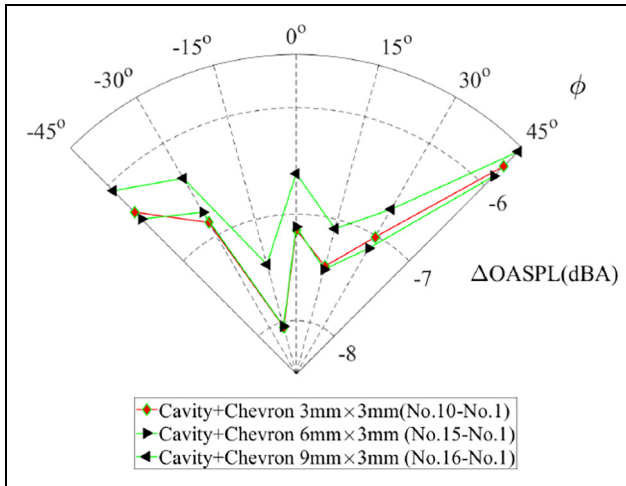


**Figure 20.** A-weighted  $\Delta$ OASPL directivity of the noise reduction, achieved using chevron with different  $a$  ( $\alpha = 90^\circ$ ).

noise reduction, which is in good agreement with the spectra in Figure 18.

Effects of the noise reduction from  $a$  and  $b$  are also evaluated in this study. Figures 20 and 21 show the  $\Delta$ SPL spectra with different  $a$  and  $b$ , respectively, referred to the case of only cavity (Run No. 1). It is worth noting that  $\alpha$  in all cases is  $90^\circ$ , and  $3 \text{ mm}$  ( $a$ )  $\times$   $3 \text{ mm}$  ( $b$ ) is the baseline test, that is, No. 10. As shown in Figure 20, it is observed that whichever  $a$  is, noise reduction can be obtained for all cases because  $\Delta$ SPL is negative. Furthermore, within 3, 6 or 9 mm, when  $a = 9 \text{ mm}$ , the reduction performance is not as good as the other two cases. As for  $a = 3 \text{ mm}$  and  $a = 6 \text{ mm}$ ,  $\Delta$ OASPL is almost the same at  $\phi = -15^\circ, 0^\circ$ . As for other directions, the two values of  $a$  have their own advantageous  $\phi$ , respectively, that is,  $-45^\circ$  for  $a = 3 \text{ mm}$  and  $15^\circ, 30^\circ, 45^\circ$  for  $a = 6 \text{ mm}$ .

Similarly, a similar analysis is depicted in Figure 21 on  $b$ . It is observed that  $b = 6 \text{ mm}$  attains better noise reduction than  $b = 3$  and  $9 \text{ mm}$ .

**Characterization of the flow field variation.** Noise reduction of the cavity can be well explained by the flow field data achieved from PIV. As shown in Figure 22, the instantaneous streamlines of case No. 10 are provided, that is, Cavity + Chevron with  $\alpha = 90^\circ$  and  $3 \text{ mm}$  ( $a$ )  $\times$   $3 \text{ mm}$  ( $b$ ) at  $0.25 \text{ Ma}$ . When compared with Figure 15, the streamlines of the leading-edge separation flow are found to rise to some extent. Moreover, in addition to those three examples in Figure 22, the authors carefully checked all 1000 streamline images from PIV for No. 10 and found that there is no incidence rate of the vortices that existed in the lower side of the shear layer in Figure 15 significantly. This means that the chevron can help break up the large-scale vortices into smaller ones. As discussed earlier, the Rossiter modes are an important contributor to the cavity noise, which can be attributed to the continuous impingement to the aft wall by the large-scale vortices. As such, the reason why chevron can reduce the cavity noise, for example, removing the peak in Figure 11, can be explained by raising the shear layer and breaking up the large-scale vortices.

**Control of the coupling noise.** Noise control of the coupling noise is discussed through the comparison between No. 17 with other cases. Overall, it is observed in Figure 23 that after the chevron is installed, when compared Cavity (No. 1) and Cavity + LG (No. 5), the noise can be suppressed in all directions; however, No. 17 still produces more noise than No. 10. In other words, in terms of OASPL, No. 1 > No. 5 > No. 10 > No. 17

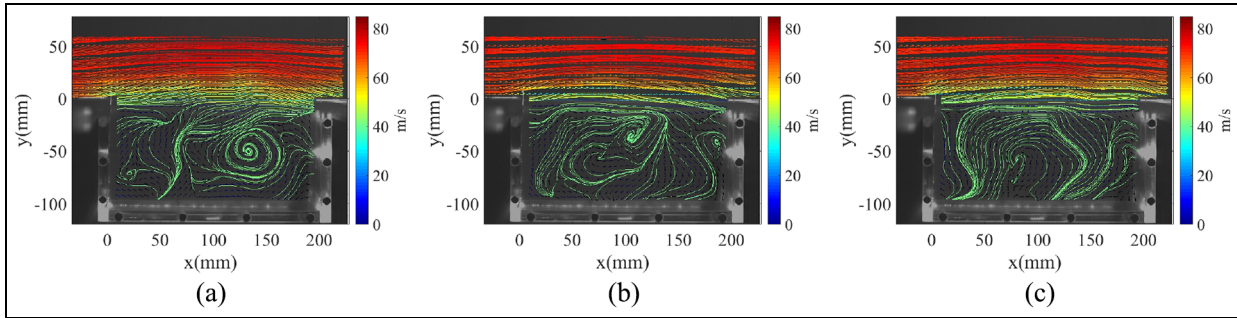


Figure 22. Examples of PIV instantaneous streamlines of the Cavity LG case (No. 10) at 0.25 Ma.

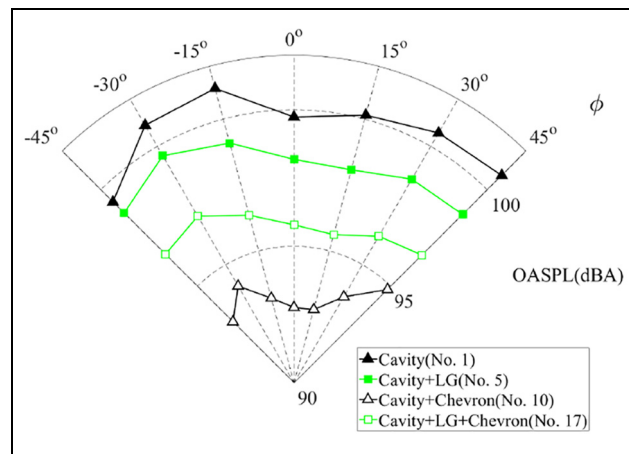


Figure 23. A-weighted OASPL directivity of cases related to the coupling noise suppression at 0.25 Ma.

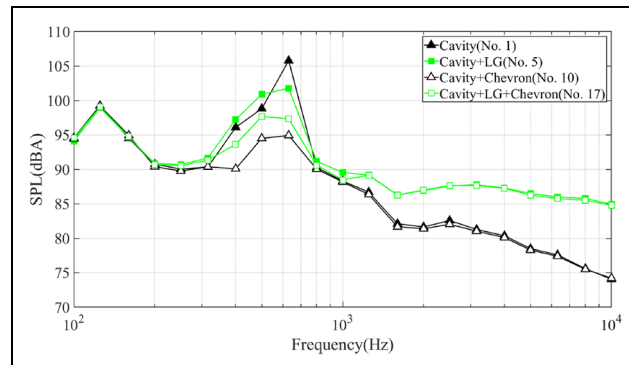


Figure 24. A-weighted 1/3 octave band spectral of cases related to the coupling noise suppression at 0.25 Ma.

(Figure 24). Since the chevron spoiler has been confirmed to be able to suppress the cavity noise, especially the Rossiter modes, even there is the LG model, the noise reduction can still be observed. Due to the fact that No. 10 > No. 17, LG model is still making non-negligible noise. However, with the spoiler, the landing

gear also produces less noise at certain frequencies. As mentioned earlier, without the chevron spoiler, the shear layer of the leading edge, which possesses large-scale vortices, will directly impinge on the LG, with much noise generated. By contrast, since the chevron spoiler elevates the shear layer and removes the

occurrence of the large-scale vortices, the impinging flow to the LG strut is modified, thereby lowering noise at certain frequencies, for example, 1250 Hz at 0.25 Ma.

## Conclusion

In this article, an experimental study was reported on characterization of the bay/landing gear coupling noise and flow, as well as the use of leading-edge spoiler to control the noise. The bay was simplified as a rectangular cavity, with a landing gear model installed. A test matrix was organised to conduct parametric investigation. Data were collected from both acoustic and aerodynamic measurements, including a 70-microphone planner array, a 7-microphone arc array, 6 pressure transducers and PIV.

Characterisation of the coupling noise and flow field was first performed. From the reduction of the SPL peak, it was found that installation of LG model can reduce the cavity noise by disturbing the formation of the Rossiter mode, that is, acoustic feedback. However, due to the 3D characteristics of the flow field, the disturbance only works on the spanwise location where the strut stays but not the whole range of the leading edge downstream field. As such, the peak only declines but not vanishes. Moreover, the frequency ranges, to which the LG model and the cavity, respectively, contributed more, are different, and the frequency range of LG model is higher than the frequency range of cavity model. In terms of the coupling noise, compared with the LG only, it was found that LG model can produce more noise at certain frequencies when the shear layer of the cavity leading edge impinges on the LG instead of  $U_\infty$ . In terms of OASPL and directivity, the clean cavity produces more noise than other cases (Cavity + LG and LG only) in all directions measured. In addition, the mean pressure distribution along the bottom of the cavity was found to be dependent on the size of the cavity, and installation of the LG will induce variation, but not much in this set-up.

For the noise suppression, the parametric study was first performed on the clean cavity. Effects from different parameters, that is,  $\alpha$ ,  $a$  and  $b$ , on the noise reduction were reported. First of all, it was observed that regardless of different parameter values, installation of the chevron spoiler can decrease the cavity noise. Similarly, from PIV results, it was found that the decrease was achieved by raising the leading-edge shear layer to prevent it from impinging on the aft edge. Moreover, there is no incidence rate of the large-scale vortices appearing along the lower edge of the shear layer after the chevron was installed. Among those parameters tested, the best value can be found when only one parameter was adjusted. This suggests that an

optimised configuration that can attain the most reduction should exist.

Finally, suppression of the coupling noise was tested, with the LG model installed. In addition to the cavity noise suppression, the chevron spoiler was also able to reduce the LG model noise in the whole set-up at certain frequencies. This is because the flow impinging on the LG model was also modified by the chevron. As such, total noise of the assembly was well suppressed by the chevron.


## Declaration of conflicting interests

The author(s) declared no potential conflicts of interest with respect to the research, authorship and/or publication of this article.

## Funding

The author(s) disclosed receipt of the following financial support for the research, authorship and/or publication of this article: This research was supported by the National Key Research and Development Program of China (grant no. 2017YFE0123300).

## ORCID iD

Kun Zhao  <https://orcid.org/0000-0003-3077-3584>

## References

1. Dobrzynski W. Almost 40 years of airframe noise research: what did we achieve? *J Aircraft* 2010; 47: 353–367.
2. Morgan HG and Hardin JC. Airframe noise—the next aircraft noise barrier. *J Aircraft* 1975; 12: 622–624.
3. Ravetta P, Burdisso R and Ng W. Wind tunnel aeroacoustic measurements of a 26%-scale 777 main landing gear. In: *Proceedings of the 10th AIAA/CEAS aeroacoustics conference*, Manchester, 10–12 May 2004. Reston, VA: American Institute of Aeronautics and Astronautics.
4. Dobrzynski W, Chow L, Guion P, et al. A European study on landing gear airframe noise sources. In: *Proceedings of the 6th aeroacoustics conference and exhibit*, Lahaina, HI, 12–14 June 2000. Reston, VA: American Institute of Aeronautics and Astronautics.
5. Ringshia A, Ravetta P, Ng W, et al. Aerodynamic measurements of the 777 main landing gear model. In: *Proceedings of the 12th AIAA/CEAS aeroacoustics conference*, Cambridge, MA, 8–10 May 2006. Reston, VA: American Institute of Aeronautics and Astronautics.
6. Zhuang N, Alvi FS, Alkislar MB, et al. Supersonic cavity flows and their control. *AIAA J* 2006; 44: 2118–2128.
7. Neri E, Kennedy J and Bennett GJ. Bay cavity noise for full-scale nose landing gear: a comparison between experimental and numerical results. *Aerospace Sci Technol* 2017; 72: 278–291.

8. Bliss DB and Hayden RE. *Landing gear and cavity noise prediction*. Technical report, NASA CR-2714, July 1976. Washington, DC: NASA.
9. Heller HH and Dobrzynski WM. Sound radiation from aircraft wheel-well/landing-gear configurations. *J Aircraft* 1977; 14: 768–774.
10. Rossiter J. Wind tunnel experiments on the flow over rectangular cavities at subsonic and transonic speeds. Technical report, RAE Farnborough, Royal Aircraft Establishment, Ministry of Aviation, London, 1964.
11. Rockwell D. Oscillations of impinging shear layers. *AIAA J* 1983; 21: 645–664.
12. Cattafesta LN, Song Q, Williams DR, et al. Active control of flow-induced cavity oscillations. *Prog Aerosp Sci* 2008; 44: 479–502.
13. Boorsma K, Zhang X, Molin N, et al. Bluff body noise control using perforated fairings. *AIAA J* 2009; 47: 33–43.
14. Li Y, Smith M and Zhang X. Measurement and control of aircraft landing gear broadband noise. *Aerosp Sci Technol* 2012; 23: 213–223.
15. Oerlemans S and Bruin AC. Reduction of landing gear noise using an air curtain. In: *Proceedings of the 5th AIAA/CEAS aeroacoustics conference*, Miami, FL, 11–13 May 2009. Reston, VA: American Institute of Aeronautics and Astronautics.
16. Zhao K, Yang X, Okolo PN, et al. Use of dual planar jets for the reduction of flow-induced noise. *AIP Adv* 2017; 7: 025312.
17. Zhao K, Alimohammadi S, Okolo PN, et al. Aerodynamic noise reduction using dual-jet planar air curtains. *J Sound Vib* 2018; 432: 192–212.
18. Shaaban M and Mohany A. Passive control of flow-excited acoustic resonance in rectangular cavities using upstream mounted blocks. *Exp Fluids* 2015; 56: 72.
19. Saddington AJ, Knowles K and Thangamani V. Scale effects on the performance of sawtooth spoilers in transonic rectangular cavity flow. *Exp Fluids* 2016; 57: 2.
20. Saddington AJ, Thangamani V and Knowles K. Comparison of passive flow control methods for a cavity in transonic flow. *J Aircraft* 2016; 53: 1439–1447.
21. Luo K, Zhu W, Xiao Z, et al. Investigation of spectral characteristics by passive control methods past a supersonic cavity. *AIAA J* 2018; 56: 2669–2686.
22. Bennett GJ, Okolo PN, Zhao K, et al. Cavity resonance suppression using fluidic spoilers. *AIAA J* 2018; 57: 1–14.
23. Arunajatesan S, Kannepalli C, Sinha N, et al. Suppression of cavity loads using leading-edge blowing. *AIAA J* 2009; 47: 1132–1144.
24. Shaw L, Clark R and Talmadge D. F-111 generic weapons bay acoustic environment. *J Aircraft* 1988; 25: 147–153.
25. Schlinker RH and Amiet RK. Refraction and scattering of sound by a shear layer (AIAA 1980-973). In: *Proceedings of the 6th AIAA aeroacoustics conference*, Hartford, CT, 4–6 June 1980. Reston, VA: American Institute of Aeronautics and Astronautics.
26. Kegerise M, Spina E and Cattafesta L III. An experimental investigation of flow-induced cavity oscillations. In: *Proceedings of the 30th fluid dynamics conference*, Norfolk, VA, 28 June–1 July 1999, pp. 347–351. Reston, VA: American Institute of Aeronautics and Astronautics.
27. Gutmark EJ, Ibrahim IM and Murugappan S. Dynamics of single and twin circular jets in cross flow. *Exp Fluids* 2011; 50: 653–663.

## Appendix I

### Notation

$a$	height of the triangle in the leading-edge chevron spoiler
$b$	width of the triangle in the leading-edge chevron spoiler
$C_p$	pressure coefficient
$d$	depth of the cavity
$dt$	time interval between the paired images in the PIV tests
$l$	length of the cavity
$U_\infty$	cross-flow velocity
$w$	width of the cavity
$\alpha$	inclination angle of the leading-edge chevron spoiler
$\phi$	angle deviating from the vertical direction in the microphone directivity arc